05

Advanced Hall Magnetometer with improved performance

© Kh. R. Rostami

Fryazino Branch, Kotel'nikov Institute of Radio Engineering and Electronics, Russian Academy of Sciences,
141190 Fryazino, Moscow oblast, Russia
e-mail: rostami@ms.ire.rssi.ru

Received January 4, 2022
Revised April 28, 2022
Accepted September 26, 2022

A sharp jump in the magnetic response near the first critical twins magnetic field H_{ic1} was generated under the combined action of a constant biased and a local oscillating damped magnetic fields on the surface of the $YBa_2Cu_3O_{7-x}$ epitaxial film. The possibility of increasing due to this jump the sensitivity of a standard Hall magnetometer from $\sim 2.5 \cdot 10^{-3}$ Gs/Hz$^{1/2}$ to $\sim 8 \cdot 10^{-7}$ Gs/Hz$^{1/2}$ in the frequency range ~ 1 kHz has been demonstrated. The range of the measured magnetic fields of the magnetometer was extended to the region of weak fields $\sim (8 \cdot 10^{-7} - 2.5 \cdot 10^{-3})$ Oe, while maintaining the accuracy and linearity of the order of $\sim 0.01\%$. To increase the sensitivity, linearity and noise sustainability the beginning of the operating point of the magnetometer was shifted to the twins values H_{ic1}. The increased spatial resolution of the magnetometer, determined by the linear dimensions of the $YBa_2Cu_3O_{7-x}$ film twins, was provided by an increase in the total magnetic field directed perpendicular to the film surfaces and the Hall transducer and reached ~ 300 nm.

Keywords: the twin high temperature superconductor, the density jump of the trapped magnetic flux, biased magnetic field, oscillating damped local magnetic bias field, two-stage Hall magnetometer.

DOI: 10.21883/TP.2022.12.55191.16-22

Introduction

Currently, much attention is paid to the study of one of the main fundamental problems of applied physics, i. e. the principles of developing alternative methods of high-precision magnetometry, the application of which can vary from medicine to the study of planetary magnetic fields [1–5]. High-precision magnetometers are also needed in chemistry and physics to study quantum mechanical processes in substances under conditions of magnetic vacuum, low temperatures, etc. To date, superconducting quantum interference devices (SQUID) of magnetic field [1,2] and magnetometers with optical pumping of alkali metal vapors with strong spin polarization [3,4] have the highest performance. These magnetometers have extremely high sensitivities $\sim 10^{-8} - 10^{-11}$ Gs/Hz$^{1/2}$ and $10^{-6} - 10^{-8}$ Gs/Hz$^{1/2}$, respectively. At the same time, these magnetometers have a low spatial resolution. Alternatively, magnetometers based on solid-state spin systems, which have extremely high spatial resolution, such as broadband ensemble NV-diamond magnetometers [5], have a sensitivity by several orders of magnitude lower than SQUID magnetometers. In this regard, in order to increase the sensitivity to the SQUID sensitivity level while maintaining the spatial resolution of NV magnetometers the developments in the field of quantum mechanical probing of diamond crystals with a nitrogen vacancy are also being actively taken. To cover the intermediate case between NV magnetometers and SQUID, on the one hand, and magnetometers with low sensitivity and spatial resolution, on the other hand, a number of magnetometers have been developed. In particular, the fields of application of the latter devices include measurements of magnetic field parameters, magnetic properties of materials, magnetic field gradients, magnetic noise levels, geological exploration, medicine, etc. To solve these problems, NMR and EPR magnetometers are used [6,7]; saturation induction magnetometers, ferroprobing magnetometers [8], Hall magnetometers [9–11], etc. are used. The above magnetometers differ from each other in their spatial resolution, signal measurement accuracy, sensitivity by the level of the recorded signal, output signal linearity, magnetic field measurement ranges, temperature sensitivity and the ability to conduct studies on objects with different spatial scales, cost, etc. Devices based on quantum phenomena, which have the lowest sensitivity threshold close to the magnetic vacuum level, are complex and expensive. NMR and EPR magnetometers with a sensitivity of $\sim 10^{-3} - 10^{-5}$ Gs/Hz$^{1/2}$ are widely used to study the structures and properties of various substances with high spatial resolution and precision. However, they specify high demands on the uniformity and stability of the magnetic field [6,7]. Since the sensor is part of a resonant circuit, this significantly reduces the field measurement range covered by a single sensor [7], and as a result, there are significant problems in speeding up signal processing and optimizing them. The above quantum magnetometers measure the increment of the magnetic field and are not devices for measuring the absolute values of constant and weakly changing magnetic fields. They have low linearity, which creates serious problems in interpreting the results obtained. The sensitivity of ferroprobing magnetometers most widely used as a meter of the absolute value of the magnetic

field at low temperatures reaches $\sim 10^{-6}$ Gs/Hz$^{1/2}$ [8]. However, despite the relative low cost and easy use, these magnetometers have low linearity and spatial resolution, since in inductive transducers high-frequency pumping and signal pickup are carried out using coils wound directly on a core made of magnetically soft material. Hall-probe (HP) based magnetometers [9–11] also provide direct measurement of magnetic field induction. Besides, they have a wide range of measured magnetic fields and functionality, allow visualization of the magnetic microstate of extended objects, have high accuracy and linearity of the output voltage, are easy to manufacture and have a low cost. However, despite these positive aspects, the sensitivity, spatial resolution, and accuracy of Hall magnetometers are insufficient for clearly distinguishing the spectrum of the signal response to a weak magnetic field of nanoparticles. In this paper, we will describe an improved magnetometer based on HP platform with extended functionality, which allows it to provide higher sensitivity and response than Hall magnetometers [12,13].

1. Physical basis for making magnetic field sensor

As it is known [14–17], high-temperature superconductors (HTSCs) have a complex crystal structure consisting of twins (monodomains, grain crystallites, sub- and nanocrystallites) interconnected by weak Josephson bonds. The studies of a more technologically accessible HTSC, i. e. $YBa_2Cu_3O_{7-x}$ (YBCO) also revealed that even the most perfect single crystals of YBCO HTSC contain a great number of regularly positioned twin boundaries (TBs) with twinning plane (110). Depending on the method of material preparation, TB width $\Delta d \approx 30-50$ Å, and distance between TBs can be $d \approx 200-2000$ Å [18,19]. TBs are well detected not only in single-crystal YBCO and in bulk polycrystalline YBCO HTSC grains, but also in YBCO epitaxial films. It was shown in papers [15–17] that with the external magnetic field increasing, the critical currents of weak Josephson junctions between twins are suppressed, and at H_{ic1} if HTSC twins the sample abruptly „divides“ into groups of twins with quantized spatial scales. Groups of twins formed during the sample „division“ are sorted by close demagnetizing factors *n*. In this case, with the external field increasing and the sample decay into smaller twins, the short-range order in the glassy crystal structure of HTSC is enhanced, which makes it possible to determine the minimum period of the TBs distribution. The sharpness of the hops increases, the value of H_{ic1} of twins increases, and the spatial resolution of the Hall magnetometer described below improves. It should be noted that the presence of TBs is in the very nature of YBCO HTSC, since twin domains form as a result of the structural phase transition from the tetragonal (nonsuperconducting) phase to the orthorhombic (superconducting) one at a temperature of ≈ 700°C and/or as a result of alteration of stoichiometry of samples induced by doping [14–20]. Since the properties of TBs are also clearly manifested in other cuprates (preferably in LaSrCuO compounds), as well as in twin, rhombic and underdoped iron pnictides — $Ba(Fe_{1-x}Co_x)_2As_2$ crystals [20], the main purpose of this paper is to demonstrate the possibility of using the property of jump-like decay of the sample into twins in twin cuprate and iron-containing pnictide HTSCs to create based on them of the improved Hall magnetometer (IHM) with increased performance.

2. Principles of making the sensor chamber and IHM

To expand the functionality, as well as achieve higher sensitivity and speed, we replaced one solenoid with two coaxial sensors in the chamber [12,13].

Fig. 1 shows the structural diagram of the magnetic field sensor chamber.

Fig. 2 shows a diagram of the control unit for the magnetic field sensor chamber and of the measuring part, which is basis for IHM making. The functioning of the IHM, which operates on the principle of the tracking system, which also includes the YBCO HTSC epitaxial film, means: first, under the command of the computer *11* or of manual control unit *10*, the adjustable DC source *3* is connected to the solenoid of the reference bias magnetic field L_1, and the field Hm is created in it. Next, the response signal created in the film is recorded using basic Hall magnetometer *1*, its output signal is fed to one of the inputs of the comparator *4*, the comparator output, in its turn, is connected to the trigger input *5*. The trigger outputs *5* are connected to the inputs of the logical multiplication circuits *7, 8*, their outputs are connected to the counting inputs of binary-decimal updown counters (BDUC). The BDUC output signals alternately switch the currents of the discharge generators of square-wave pulses *2* of arms of positive 9_1 and negative 9_2 polarity. The outputs of the arms of the positive and negative polarity of the current of the bipolar source are connected through the chokes to the inputs of the current switches and through the resistors R_1, R_2 to the second input of the comparator *4*. Under the computer command *11*, the outputs of the current switches alternately connect through a capacitance *C* and a resistor *R* the outputs of the discharge current generators of the positive and negative polarity arms of the bipolar source to the inputs of the bias field solenoid. Thus, the oscillating damped local magnetic field (ODLMF) (the bias field) created in the magnetic field transducer chamber is summed with the reference bias magnetic field. The bias field is created as follows: when pulses from the computer *11* are received in the current arm of positive polarity, a low-current adjustable bipolar current source *2* is connected through the current switches to a solenoid L_2, which creates the bias field. Thus, the magnetic energy is accumulated in the solenoid. When changing the polarity of the pulses coming from the comparator *4* to the current

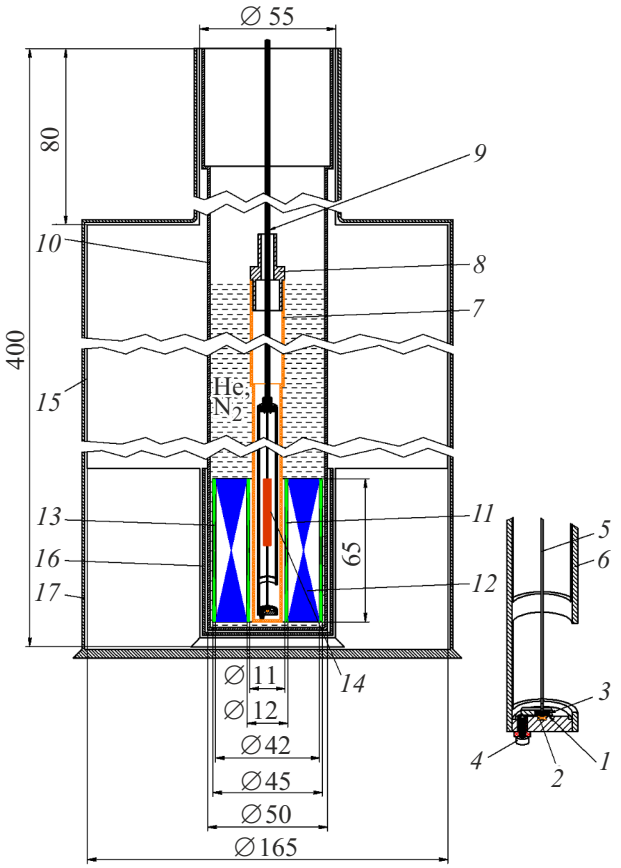

Figure 1. Structural diagram of the magnetic field sensor chamber: *1* — HTSC epitaxial film, *2* — HP, *3* — sample, *4* — brass contact screw, *5* — copper rod, *6* — copper guide cylinder, *7* — ebonite cap (ampoule), *8* — stainless rod, *9* — stainless tube, *10* — lower narrowed part of the cryostat, *11* — bias field solenoid, *12* — reference magnetic solenoid displacement field, *13* — compensation field solenoid, *14* — heater, *15* — main part of cryostat for main refrigerant capacity, *16* — superconducting shield, *17* — outer magnetic shield.

switches using the logical multiplication circuit *7*, the positive polarity current arm of the low-current bipolar current source *2* of the bias field solenoid is switched to the resistor R and the capacitance C is connected into the solenoid circuit L_2. This leads to the capacitor C charging and to the magnetic energy transformation into electrical energy. As a result of successive transformations of the magnetic energy into electrical energy, and vice versa, in the L_2C-circuit an ODLMF of positive polarity occurs, which is described by the equation

$$H_1(t) = H_{o1} \exp(-\beta t) \cos \Omega t, \qquad (1)$$

where $\beta = r_2/(2L_2)$ — damping factor, $\Omega = (\omega^2 - \beta^2)^{1/2}$ — natural frequency of the oscillatory circuit, $\omega^2 = 1/(L_2C)$, r_2 — residual resistance of the solenoid L_2 for cases when the coil is wound from a non-superconducting wire. When a pulse is received from the comparator *4*, which gives permission to change the polarity of the output voltage of the bipolar source *2*, the current arm of the negative polarity is connected to the current switches using the logical multiplication circuit *8*, and through the solenoid L_2 reverse current begins to flow. In this case, the magnetic energy accumulation in L_2, as well as the charging and discharging of the capacitance C proceed similarly to the method described above. As a result, a high stable, uniform, negative-polarity ODLMF is created in L_2 solenoid.

By switching the output voltages of the source *2* in L_2 solenoid, a high stable bipolar homogeneous ODLMF is created

$$H_1(t) = \sum_{i,j=0}^{N} (H_{01i} - H_{01j}) \exp(-\beta t) \cos \Omega t. \qquad (2)$$

Here H_{01i}, H_{01j} is given strength of magnetic bias fields, t is time, $i, j = 0, 1, 2, \ldots N$, where N is the number of steps specified by the amplitude $H_{01} \exp(-\beta t)$ of the ODLMF.

The field H_m of the solenoid *12* (Fig. 1) $L_1 \approx 0.52$ H can vary over a wide range $\sim 1-150$ Oe.

The second solenoid of the bias field *11*with a low inductance $L_2 \approx 0.049$ H made it possible to create a weak ODLMF with a frequency of more than 500 kHz and an amplitude of up to 3 Oe.

Thus, the summary field created by two coaxially located solenoids is applied to the YBCO epitaxial film in superconducting state perpendicular to the surface:

$$\sum H(t) = H_m + H_1(t) = H_m + H_{01} \exp(-\beta t). \qquad (3)$$

The film disintegrates abruptly into groups of twins with close n when the field amplitude reaches the values of the fields of H_{ic1} twins. This, in its turn, leads to abrupt penetration of the magnetic flux into the film through the TB, causing a jump effect on the magnetic field dependence of the trapped flux (TF) density — $B_{tr}(H_0)$ in HTSC films [15–17].

Fig. 3 shows the dependences of $B_{tr}(H_0)$ YBCO epitaxial films obtained in a similar technological cycle. The measurements were carried out using the proposed IHM. Fig. 3, *a* shows the dependencies for the large step ΔH_0; Fig. 3, *b* and the insert in Fig. 3, *a* show the dependences of $B_{tr}(H_0)$ YBCO epitaxial films for small step of ΔH_{01} value change in the region of jumps. As can be seen from Fig. 3 that jumps in the dependences $B_{tr}(H_0)$ for different YBCO epitaxial films occur at approximately the same H_0 values.

3. Algorithm of actions of IHM measuring part

As shown in [21], YBCO HTSCs are controlled reversible storage media. This allowed to control the process of multiple recording and erasing of TF density in the film by the summary field, i.e. by reference magnetic bias field and by the amplitude $H_{01} \exp(-\beta t)$ of the weak ODLMF.

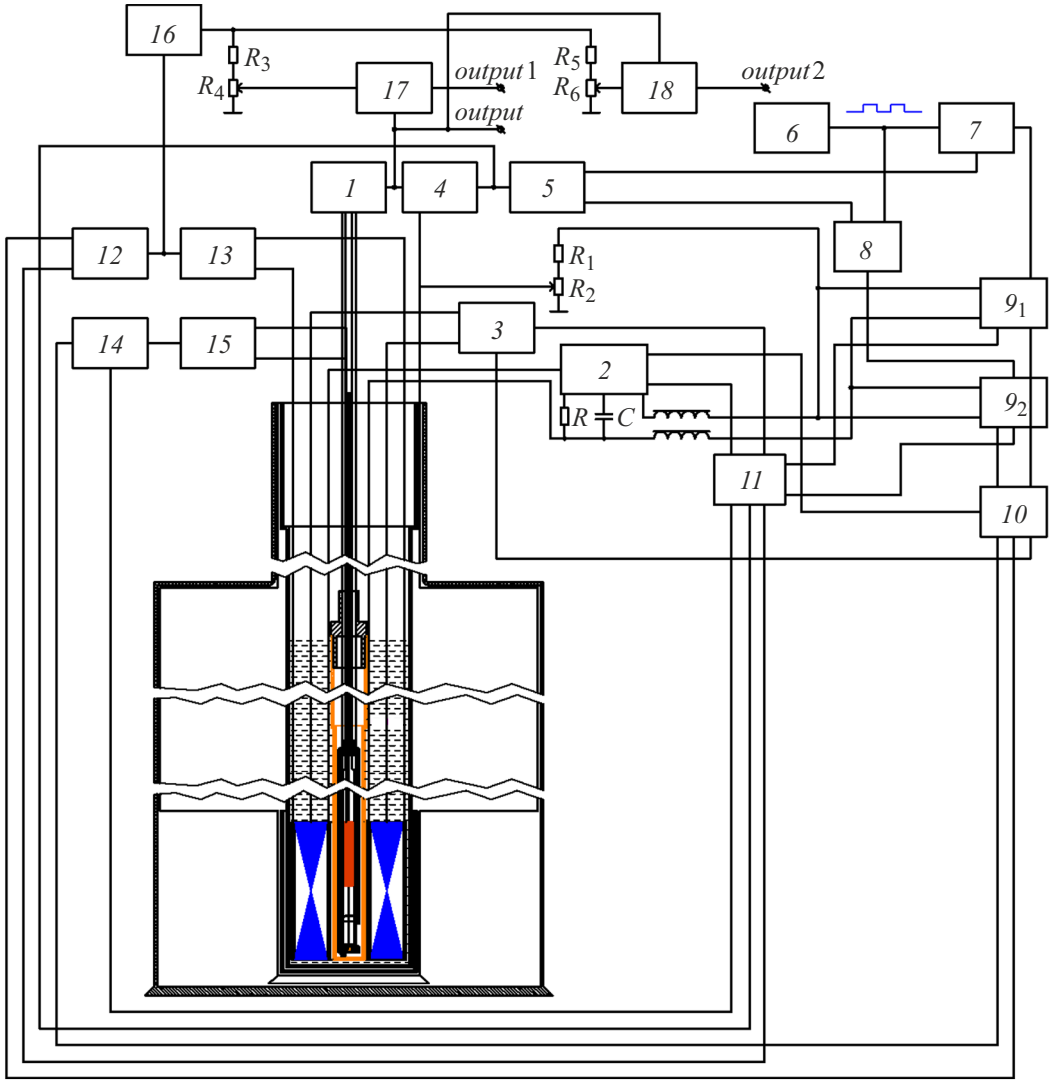

Figure 2. Block diagram of two-stage magnetometer implementing the proposed method: *1* — Hall magnetometer, *2* — discharge generators of square-wave pulses, *3, 13, 15* — regulated DC sources, *4, 17* — comparators, *5* — trigger, *6* — square wave generator, *7, ,8, 12, 14* — circuit of logical multiplication, $9_1, 9_2$ — current arms of positive and negative polarity, *10* — manual control unit, *11* — computer, *18* — differential amplifier.

When two coaxial solenoids L_1 and L_2 pass through the inner hole, the studied weak magnetic fields are added to the strong threshold reference bias field and the weak bias field and are amplified by them. When the condition is met

$$H_m + (q - p)H_{01} + |H_p| = H_{ic1} \qquad (4)$$

in the film there is abrupt change in its residual differential magnetic permeability $\Delta\mu_{tr} = \Delta B_{tr}/\Delta H_{01} \approx 0.2$ (Fig. 3) and, thus, the value of the amplified signal is registered with the help of HP. To establish the value of the desired field $|H_p|$, the value of the reference bias field H_m was chosen from the condition

$$|H_{ic1} - H_m|/H_{ic1} \ll 1. \qquad (5)$$

The peak value of the amplitude of the desired field $|H_p|$ was measured after adding to it the selected value H_m and the amplitude $H_{01}\exp(-\beta t)$ of ODLMF varying in narrow band ΔH_0 by fitting the $(qp)H_{01}$ value and implementing the condition (4). Then $|H_p|$ value was determined from equation (4). $\Delta H_0 \approx 4.66$ Oe value corresponds to the minimum change step H_m (so that $\Delta H_0 \ll H_m$). In the equation (4) q and p are the number of the changes in the number of steps H_{01} and represent the measure of adding or subtracting the field H_{01} to the left side of the equation (4) until reaching the exact value H_{ic1}. The process of fitting the left side of equation (4) to its right side is illustrated by the diagram shown in Fig. 4. q and p values are registered by the computer *11*(Fig. 2). As can be seen from formulas (4) and (5), that for a fixed H_{ic1} and change in the external magnetic field in the range

$$H_m \le H_o \le H_m + (q - p)H_{01} \qquad (6)$$

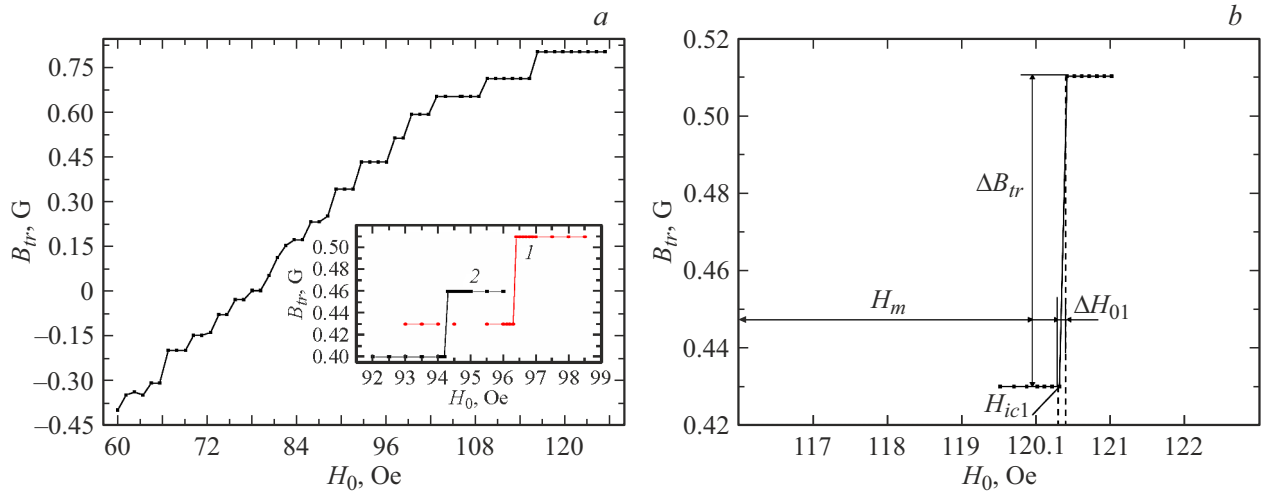

Figure 3. *a* — dependences of $B_{tr}(H_0)$ YBCO epitaxial films obtained in a similar technological cycle. The insert shows the dependences for a small step of H_0 value change in the region of jumps; *b* — dependence of $B_{tr}(H_0)$ YBCO epitaxial film at a small step of H_0 value change in the region of jumps.

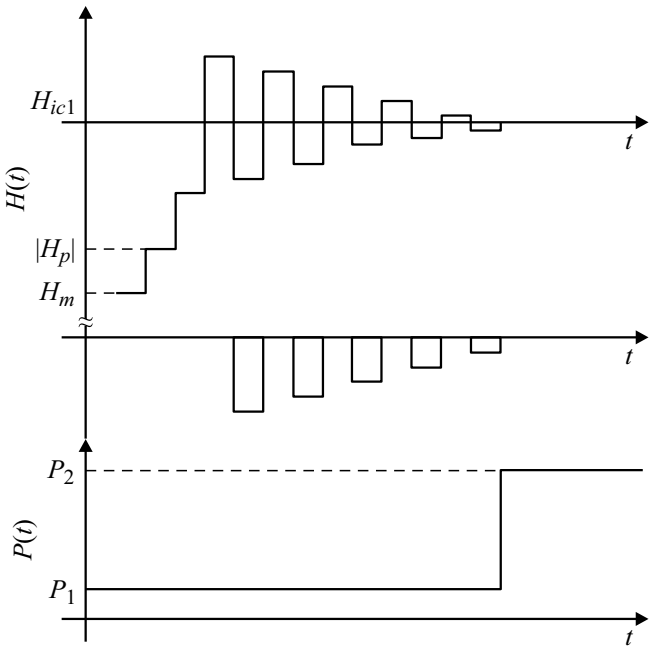

Figure 4. Diagram of the operation of the IHM.

It is possible to register weak magnetic fields with high sensitivity. By choosing sufficiently large values H_{ic1} and varying H_m in a wide range according to formula (4), one can create a wide-range magnetometer. Besides, the fulfillment of the conditions

$$\Delta H_{01}/\Delta H_0 \ll 1; \quad \Delta H_0/H_m \ll 1, \tag{7}$$

i. e. selective narrowing of the measurement area significantly increased the linearity, accuracy, and noise immunity of the magnetometer. To ensure equal high performance of the medium (consisting of coaxial solenoids L_1 and L_2, YBCO-film, tracking system and HPs), amplifying and recording H_P, a wide range of measured fields of the measuring part of the sensor chamber was discretely divided into three sections, in each of which the accuracy, linearity, stability, and frequency of the magnetometer were selected according to the signal level. In the rough limit for the signal with a higher level, the measurement frequency increases, and the accuracy and linearity of the magnetometer increase. At the same time, in each of the three measurement ranges the value of the H_{01} steps changed by the same value at regular time intervals t.

Since it is necessary to register weak magnetic fields, in this case it is very important to consider the issues of minimizing the errors of the magnetometer with HP and to ensure high linearity and low zero drift of the magnetometer. Note that the occurred circuit errors of the magnetometer are mainly associated with the following factors: errors of the elements of external circuits; accuracy of the elements connected in the magnetometer circuit, tolerances of resistors, capacitor leaks, thermal drifts and noise of operational amplifiers and HPs, accuracy of the gain of the operational amplifiers, errors of the operational amplifiers, stability of the output current of the HP power supply developed in [9], the accuracy of the HP residual voltage compensation, and the precision of the phase shifter of the Hall magnetometer. The errors are also related to the input voltage shift of the operational amplifier and the finite rate of rise of the output signal of the operational amplifier [22], which are part of the compensating circuit and the scale differential amplifiers of the magnetometer. To reduce the errors and to solve the above problems, it is much more correct to shift the working point of the magnetometer HP to the region of strong magnetic fields (where both the HP and the magnetometer have better linearity and accuracy), and only after that weak recorded magnetic field can be applied to it. To reduce

the effect of drift and instability of the amplifier and to create the possibility of accurately measuring a small change in a large signal, the search system made in the proposed magnetometer automatically finds the working (zero) point of the magnetometer. This allows, after registering a certain value of the input signal, to amplify its subsequent deviation from this level with a strictly specified gain. Thus, a small deviation of the measured field value is first registered and then amplified. The developed precision circuit for the HP signal registration, which operates stably over time and with temperature change, is described in [9] and can, in principle, allow the signal registration at a level close to the minimum threshold Hall EMF of HP. Such a high sensitivity can be achieved by a high temperature-stable element base of the electronic part of the magnetometer and using a precision operation amplifier of 140UD24 type or its foreign analogues in the preliminary circuit. To remove noise from the signal and to process it, it is necessary to use an automated wavelet transform method.

The frequency range of the measured fields is discretely divided into subranges, where the magnetometer parameters are rigidly fixed. In each subrange, due to the mutual compensation of positive and negative half-periods of the ODMLF oscillations, it is possible to achieve an average zero level of noise of all types. At helium temperatures, the internal fields of substances located near the surface of the film with HP were measured by the magnetometer operating in a closed mode, at that the measuring part of the sensor chamber being placed inside a superconducting screen, and the entire system was located inside a cylindrical magnetic screen made of aluminum and permalloy. In the case of nitrogen temperatures, when the superconducting screen passed into the normal state, the Earth's magnetic field and all possible pickups are screened by the external large screen. If the magnetometer is used as an open system, the inner and outer magnetic shields were not used, and the Earth magnetic field was compensated using the solenoid of the third outer section of coaxial solenoids with inductance $L_3 \approx 0.049$ H. This compensation was carried out by passing through the solenoid L_3 of the constant current of regulated source *13* controlled by the logical multiplication circuit *12* and the computer *11*. To register in space of weak constant and variable magnetic fields, the magnetometer for such open system worked as an „antenna". The measuring wires passed between coaxial thin stainless steel tubes of the central rod *7* (Fig. 1). Note that due to the stepwise change of the amplitude $H_{01}\exp(-\beta t)$ of ODMLF, a situation of a smooth transition from large to small spatial scales is created. This is achieved by gradual decreasing of steps height of $H_{01}\exp(-\beta t)$ field from $\Delta H_0 \approx 4.66$ Oe to the minimum $\Delta H_0 = 0.1$ Oe, while after each cycle of measurements the film was heated to a temperature above T_c using a substrate heater *14* (Fig. 1) and then cooled again to temperature of $T = 77.4$ K. The control using tracking system of the size of the steps of ODMLF applied to the H_{01} film with $H_{01}\exp(-\beta(t=0))$ amplitude made it possible to control the process of multiple reverse recording and erasing of the TF density [21]. This made it possible to simultaneously use the film as a sensitive element and as an important component of the tracking system. At the same time, the application of the procedure dividing the range of measured fields into a wide area of the reference displacement field H_m (HP zero point shift) and a weak bias field formed the basis of technical, technological and design solutions when developing the proposed magnetometer.

Fig. 4 shows a diagram of the operation of the IHM. The operation algorithm was as follows: first, the film in a zero magnetic field was transferred to the superconducting state with the power supply of the heater *15* switched off using the computer *11* and the AND circuit *14* (Fig. 2), then a step of the reference magnetic displacement field $H_0 = H_m$ was applied. After the field was removed, the TF density — B_{tr1} of the film was measured with HP, and the signal P_1 was set at the output of the comparator *4* (Fig. 2). This method was used to measure the magnetometer gain K_1 before the jump in the magnetic response of the YBCO film to the magnetic field. The obtained data were entered into a computer *11*. Next, a bias field, i. e. ODLMF was superimposed on the reference displacement field H_m:

$$H_0 \le H_m + H_{01}\exp(-\beta t) \le H_{ic1} \tag{8}$$

and at the same time access of the measured magnetic field H_p to the film was provided. If

$$H_0 = H_m + H_{01}\exp(-\beta t) + |H_p| > H_{ic1} \tag{9}$$

the pre-set value at the output of the comparator *4* changes (Fig. 2), the polarity of the power supply of the bias field solenoid is switched, and the unit operation returns to its original state. Then step $H_{01}\exp(-\beta t)$ of a lower level was applied so that

$$H_m + H_{01}\exp(-\beta t) + |H_p| \le H_{ic1} \tag{10}$$

and the search procedure continued until condition (4) was implemented, and the comparator *4* output had jump from the P_1 state to the P_2 state. The measured updated value of the parameter B_{tr2} was also entered into the computer *11* (Fig. 2), and the magnetometer gain was determined with abrupt jumps of the magnetic response of the film to the reference displacement magnetic field and the bias field of ODLMF. Thus, the resulting gain of the developed IHM was determined from the formula

$$K = K_1\left(\frac{H_m}{\Delta H_0}\right)\left(\frac{\Delta H_0}{|H_{ic1} - H_m|}\right) = K_1\,\frac{H_m}{(q-p)H_{01}}. \tag{11}$$

Since the magnetic response of the film is proportional to the peak value of the measured field H_p, the value H_p was determined by the difference between the measured values:

$$|H_p| = \frac{\Delta B_{tr}}{K} = \frac{B_{tr2} - B_{tr1}}{K_1\frac{H_m}{(q-p)H_{01}}} = \frac{(B_{rt2} - B_{tr1})(q-p)H_{01}}{K_1 H_m}. \tag{12}$$

4. Method of film synthesis and magnetometer parameters

Cylindrical YBCO epitaxial films with a diameter of 8 mm, thickness h up to 1 μm, and axis **c** oriented perpendicular to the substrate surface were also fabricated by laser sputtering on $NdGaO_3$ (110) substrate of a stoichiometric high-density YBCO target. The critical temperature of the transition to the superconducting state measured by the inductive method is $T_c \approx 92$ K, and the width of the superconducting transition is $\Delta T_c \approx 0.6$ K. The active resistance of the solenoid L_1, wound using PETV-943 copper wire with diameter of $\Phi = 0.25$ mm, was $r_1 \approx 20\,\Omega$ at a temperature of 77.4 K. The active resistances of the solenoids L_2 and L_3, wound using PETV-943 copper wire with diameter of $\Phi = 0.17$ mm, were $r_2 \approx 2.2\,\Omega$, $r_3 \approx 2.2\,\Omega$ at 77.4 K. The capacitance of the capacitor connected in parallel to the inductance L_2 was $C \approx 0.1\,\mu$F. Oscillation damping coefficient $\beta \approx 22\,s^{-1}$, natural frequency of the oscillatory circuit is $f \approx 500$ kHz. In parallel with the solenoid L_1, a capacitor $C \approx 0.3\,\mu$F was connected. In this case, the oscillation damping coefficient is $\beta \approx 20\,s^{-1}$, and for the oscillatory circuit L_1C the natural frequency is $f \approx 10$ kHz. The fields H_m and $H_{01}\exp(-\beta t)\cos\,\Omega t$ were switched synchronously with the frequency of $f \approx 1$ kHz. To ensure the magnetometer operation at higher frequencies, as well as in the pulsed mode, it is necessary to use high-frequency sensors instead of the standard HP. The magnetometers [12,13] had no solenoid L_2, and the bias field of ODMLF was created by the solenoid L_1. In this case, instead of (4) the condition was implemented

$$H_m \exp(-\beta_1 t)\cos\,\Omega_1 t + |H_p| = H_{ic1}, \qquad (13)$$

which resulted in $\Delta\mu_{tr} = \Delta B_{tr}/\Delta H_0 \approx 0.02$ (Fig. 3, *a*) decreasing by an order of magnitude. This, in turn, significantly decreased the degree of response of the tracking system. Since the inductance of the solenoid L_1 is by an order of magnitude greater than the inductance L_2, the response in the proposed magnetometer turned out to be by an order of magnitude better than in magnetometers [12,13]. The magnetometer response was limited by the rate of relaxation of the measured TF density in the film. Due to the fact that after the removal of the ODMLF step applied to the film the positive and negative half-periods of the tail part of TF are mutually compensated, the vortices and antivortices generated by these half-periods quickly annihilate, preventing the vortices exit from the film, and thereby stopping the process of magnetic relaxation in it. Switching the ODMLF steps using tracking system of polarities with $H_{01}\exp(-\beta t)$ amplitude also resulted to a hard temporal fixation of the TF density. As can be seen from Fig. 3, within 5 min after the ODMLF step removal the values B_{tr} between the steps do not change.

5. Results obtained and discussion

In Fig. 3, the following parameters for an epitaxial film of thickness $h \approx 0.5\,\mu$m turned out to be equal to: $H_{ic1} \approx 120.252$ Oe, $\Delta B_{tr} \approx 0.082$ Gs, $\Delta H_0 \approx 4.66$ Oe, $\Delta H_{01} \approx 0.1$ Oe. H_{ic1} value is the sum of the fields $H_m \approx 120$ Oe, and ODMLF ≈ 0.252 Oe. The current through the solenoid L_2 created by the discharge generators 9_1 and 9_2 (Fig. 2), was given by binary code. The generators are a current digital-to-analogue converter (DAC), in which the current of each discharge is stabilized with an accuracy of 0.01% minimum [23]. The above data correspond to the field value H_{ic1}, which was measured at liquid nitrogen temperature and did not change during long-term experiments. Such characteristics ensured sensitivity to the summary field in the sensor chamber $K \approx 8 \cdot 10^{-7}\,\text{Gs/Hz}^{1/2}$ (see below), which is by more than an order of magnitude higher than the sensitivity of magnetometers [12,13]. In this case, the sensitivity K_1 of the developed basic magnetometer was $\approx 2.5 \cdot 10^{-3}\,\text{Gs/Hz}^{1/2}$ [9]. The range of measured fields of the magnetometer was $(8 \cdot 10^{-7} - 2.5 \cdot 10^{-3})$ Oe. The spatial resolution of the magnetometer is determined by the linear dimensions of the twins, which in the field $H_{ic1} \approx 120.252$ Oe were $a_g = (\Phi_0/H_{ic1})^{1/2}$ $approx 300$ nm. Here $\Phi_0 \approx 2.07 \cdot 10^{-7}\,\text{Gs}\cdot\text{cm}^2$ is the magnetic flux quantum. Besides, the spatial resolution of the magnetometer also depends on the twins distribution spectrum and on the magnetometer sensitivity [15,16]. The 3D scanning Hall microscope developed in [24] makes it possible to map in the homogeneous field the distribution of weak fields with a resolution of 1 μm, but when applying ODMLF to the object under study an even higher resolution $\approx 0.081\,\mu$m can be achieved [15,16]. Shifting the work point of the Hall magnetometer using H_m field is similar to voltage shifting in precision amplifiers and allows not only the accuracy and linearity increasing, but also expansion of the magnetometer measurement range by adjusting H_m in the range 0–150 Oe. Fitting $(qp)H_{01}$ in a narrow measurement range ΔH_0 (see equation (4)) made it possible to significantly shift the measurement range of the proposed magnetometer to the region of weak fields in the range $(8 \cdot 10^{-7} - 2.5 \cdot 10^{-3})$ Oe. As a rule, it is considered that the wider the measurement range is, the lower the measurement accuracy is, and vice versa — in a narrow range the accuracy is higher. But in the proposed method, as will be shown below, the accuracy is higher than 0.01%, and yet it does not depend on the range of measured fields, since the level of the recorded signal $|H_p|$ varies in the range ΔH_0, which in turn is $\ll H_{ic1}$. A wider measurement range in the region of weak fields and the simultaneous provision of high sensitivity and accuracy of the magnetometer are also necessary in the case of measuring the magnetic fields of biological objects, where both the first and second are necessary for the repeatability of the results obtained. To estimate the

magnetometer sensitivity, first, at a relatively high current, a constant (current-field) of the coil L_1 was established using calibrated HP, and then, at a known current the field value was determined, and the magnetic sensitivity of the magnetometer was calculated. Further, after determining the sensitivity of the basic magnetometer for current by three orders of magnitude less than the current flowing through the solenoid L_1, the constant (current-field) of the coils L_2 and L_3 was determined. Then, at a known current the field value was determined and the magnetic sensitivity of the magnetometer to the fields of the solenoids L_1 and L_2 was calculated. The input signal corresponding to the field H_p was created using solenoid L_3.

Fig. 5, *a* shows the comparator output signal *17*, to one of its inputs using resistors R_3 and R_4 through the amplifier *16* the reference signal proportional to the current was fed; and through L_3 the magnetometer output signal was fed to the second input. When equalizing the signals, the output signal of the comparator *17* jumped from the state U_1 to the state U_2. The set value of the threshold signal corresponded to the field value $\approx 8 \cdot 10^{-7}\,\mathrm{Gs/Hz^{1/2}}$. To determine the studied field H_p directed at an arbitrary angle to the film surface, its components were measured directly on the surface and around the sample. For this, three HPs with identical technical characteristics were placed on three strictly mutually perpendicular faces of a small cube, which was fixed on a copper substrate. Thus, three components H_{px}, H_{py}, H_{pz} were measured, and then the field value $H_p = (H_{px}^2 + H_{py}^2 + H_{pz}^2)^{1/2}$ of arbitrary direction was determined. In this way, we measured all the magnetic field tensors — the main elements of the magnetic field gradient matrix H_p:

$$Hp_{x,y,z} = \begin{vmatrix} \frac{\partial Hp_x}{\partial x} & \frac{\partial Hp_x}{\partial y} & \frac{\partial Hp_x}{\partial z} \\ \frac{\partial Hp_y}{\partial x} & \frac{\partial Hp_y}{\partial y} & \frac{\partial Hp_y}{\partial z} \\ \frac{\partial Hp_z}{\partial x} & \frac{\partial Hp_z}{\partial y} & \frac{\partial Hp_z}{\partial z} \end{vmatrix}. \qquad (14)$$

If H_p is directed perpendicular to the film surface with HP, then its value is maximum. To achieve a higher spatial measuring resolution of H_{ic1} nanocrystallites, it is necessary to install piezoelectric transducers on the head of the moving mechanism of the microscope [24]. In such cases the sizes of their working surface can be similar to the sizes of sub- and nanocrystallites (10−300) nm [15,16]. Such high spatial resolution exceeds the spatial resolution of converters based on heterojunctions with 2D electron gas with a working surface size of $\approx 0.3 \times 0.3\,\mu$m. Besides, as shown in [15,16], in this case each nanocrystallite can capture one magnetic flux quantum, and the jumps in the magnetic field dependence of TF density at field H_{ic1} in Fig. 3 will become more evident. The magnetometer sensitivity in this case will increase by more than an order of magnitude and can reach $K \approx 10^{-8}\,\mathrm{Gs/Hz^{1/2}}$. This exceeds the sensitivity of ferroprobing magnetometers, and, moreover, in comparison with them, it will have linearity and spatial resolution better by orders of magnitude. Due to three factors, namely, the shift of the origin of the work point of HP (in this case, up to $H_{ic1} \approx 120.252\,\mathrm{Oe}$), the narrowing of the HP operation range in the region of $\Delta H_0 \approx 4.66\,\mathrm{Oe}$ (Fig. 3), and the implementation of dependence (4) the nonlinearity coefficient turned out to be less than 0.01% (which was mainly set by HP nonlinearity) and did not depend on the achieved high sensitivity and accuracy of the magnetometer in the entire measurement range.

To determine the nonlinearity coefficient of the magnetometer the current strictly linearly increasing in time passed through the solenoid L_3, and the field value was measured.

Fig. 5, *b* shows the time dependences of the magnetometer output signal and the amplifier output voltage *16*, which is proportional to the current through the solenoid L_3, the output voltage with the help of resistors $R_{\{}5\}$ and R_6 is fed to the second input of the differential amplifier *18*.

Fig. 5, *c* shows the time dependence of the differential amplifier output signal *18*, determined by the difference between the output voltages of the magnetometer and the amplifier *16*. According to the degree of deviation of the current and field linearity, as well as to the zero signal level at the differential amplifier output *18*, it was found that the nonlinearity coefficient of the amplifying medium in the region of weak fields is $< 0.01\%$ and decreases with signal level increasing. So, a linear high-precision amplifying medium was created for recording weak magnetic fields. Compared with other methods, the advantage of the proposed one is that the measured value was determined using tracking search system that allows you to change the amplitude of the field step $H_1(t)$, according to formula (9), and by adjusting the reference field to implement formula (4) with high accuracy. Due to the fact that ODMLF steps $H_{01}\exp(-\beta t)$ were set using high stable discharge generators [23], the stability and accuracy of the magnetometer increased significantly, since the number of discharges corresponding to the measured field, was recorded with high accuracy. For a more accurate determination of H_{ic1} values, a quantitative analysis of the results obtained was also carried out. The processing of the measurement results showed that H_{ic1} value increases almost linearly with field increasing. This means that with twins size decreasing in the glassy structure of the YBCO film, the short-range order increases, their arrangement becomes more uniform, and the critical currents approach each other. Therefore, when choosing the twins group with corresponding n, it is first of all necessary to determine groups for which the abrupt jump of TF density occurs at the highest values of H_{ic1}.

Thus, despite the fact that the techniques and technologies developed by us are at the stage of development, the results obtained already now allow us to make quite optimistic forecasts when estimating the limit values of such magnetometer parameters as sensitivity, linearity, accuracy, response, and spatial resolution. In particular, considering that:

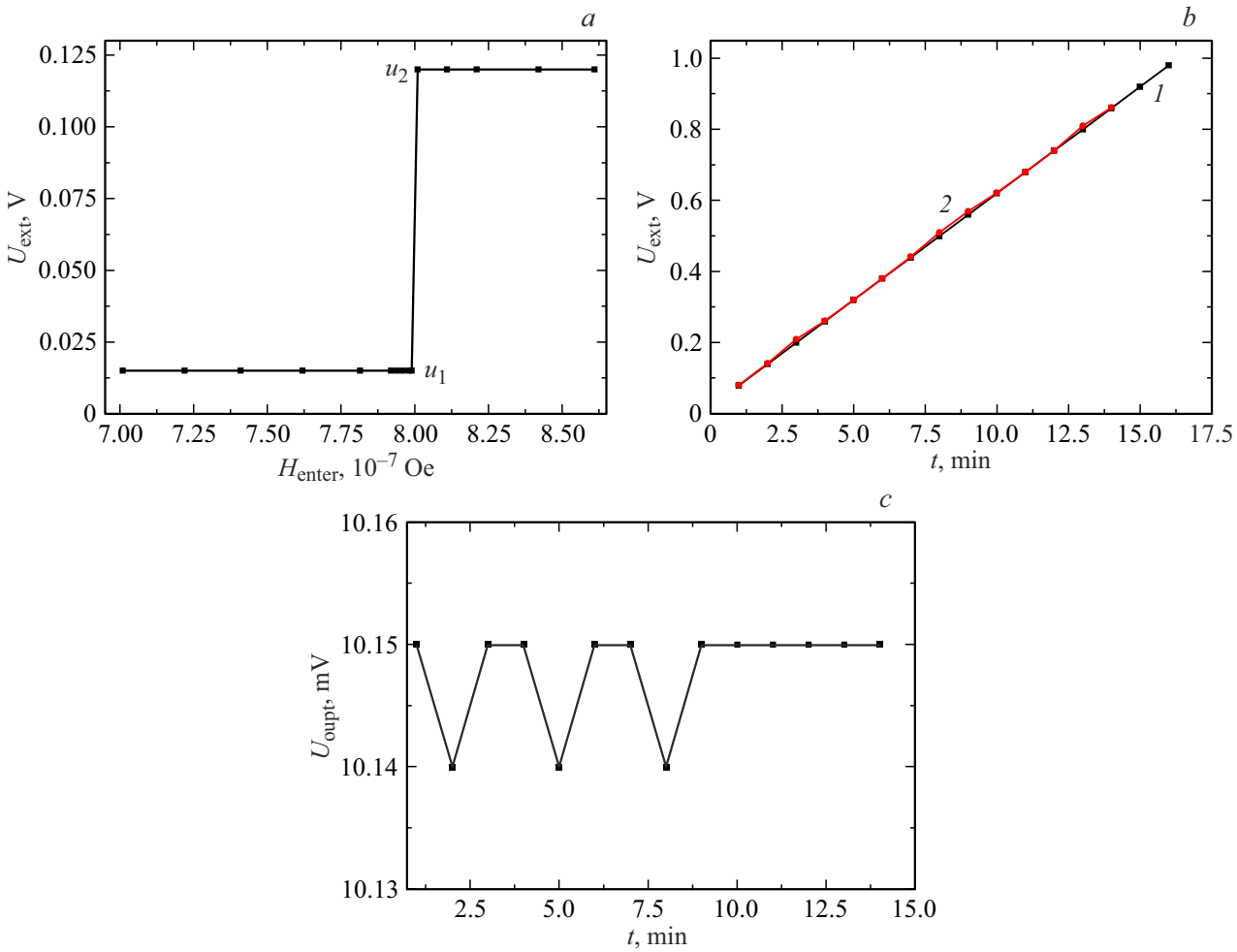

Figure 5. *a* — output signal of the comparator *17*, to one of its inputs the reference signal proportional to the current through L_3 was supplied, and to the second input the output magnetometer signal was supplied; *b* — time dependences of the magnetometer output signal (curve *2*) and the amplifier output voltage *16* (curve *1*); *c* — time dependence of the differential amplifier output signal *18* corresponding to the difference between the output signals of the magnetometer and the amplifier *16*.

a) the minimum sizes of twins can reach $d \approx 20$ nm [15,16] (may be less);

b) due to the demagnetizing factor of the film, at a temperature of ≈ 77.4 K H_{ic1} twins can reach $\sim 10^4$ Oe, and at 4.2 K $\sim (5-10) \cdot 10^4$ Oe;

c) the sensitivity of the basic Hall magnetometer can be $\sim 10^{-4}$ Gs/Hz$^{1/2}$ (see [10] and references therein);

d) the effective area of the working surface of HPH — S_{eff} is less than the set size of the working surface of the HP — S;

e) the sensitive zone of HP is located mainly in a narrow band near the Hall contacts [25];

f) $H_m/\Delta H_0 \approx 10^2-10^4$, $(q-p)(\Delta H_0/\Delta H_{01}) \approx 10^3$,

then we can conclude that the IHM sensitivity can reach $\sim 10^{-9}-10^{-11}$ Gs/Hz$^{1/2}$ and higher at spatial resolution $\sim 10-20$ nm, while having a high degree of linearity, accuracy and response. Magnetometers with such sensitivity values approach the SQUID sensitivity, but surpass them in other parameters. So, based on the results obtained, we can make the following assumptions and estimates. Since the value of the resulting gain of the developed magnetometer directly depends on the conversion coefficient of the magnetic field converter and the base magnetometer (see formula (12)), then if at the first stage SQUID-based magnetometer is used, which provides sensitivity $\sim 10^{-8}-10^{-11}$ Gs/Hz$^{1/2}$, then at the second stage the sensitivity value can also be multiplied by $\sim 10^{-2}-10^{-4}$ Gs/Hz$^{1/2}$. Besides, as shown in [26], SQUID sizes can be reduced to 100 nm. Such limit sensitivities of the magnetometer are very important for high-precision local and selective study of quantum-mechanical processes in substances under conditions of magnetic vacuum and low temperatures at the spatial resolution of the magnetometer ~ 20 nm.

One of the main problems on the way of further parameters improvement of the magnetometer is the temporal stability and repeatability of the characteristics of the films depending on their service life, which requires

periodic annealing of the film in oxygen atmosphere and re-setting of the magnetometer. The well-tested circuit diagram of the magnetometer, assembled using inexpensive discrete element base of domestic production, operated reliably for many years. To ensure high response over the entire measurement range, it is necessary to use a more computerized magnetometer circuit using high-frequency multifunctional large integrated circuits. The solution of these difficult problems requires further technical and technological developments. Also note that the proposed magnetometer can be widely used to solve many problems in various fields of science, technology and medicine, and regardless of the field of application of the magnetometer the scientific results obtained with its help will be of priority.

Conclusion

Thus, using a YBCO epitaxial film (having a sharp jump in the magnetic response to the action of the summary field at H_{ic1} twins) as a sensitive element of the magnetic field converter and simultaneously as a reversible storage medium, we demonstrated the possibility of additional increasing of the limit values of the main parameters of classical magnetometers. Thus, using as the basic magnetometer of the first stage the classical magnetometer operating on the usual Hall effect with a sensitivity of $\approx 2.5 \cdot 10^{-3}\,\mathrm{Gs/Hz^{1/2}}$ in the range of measured fields $(2.5 \cdot 10^{-3} - \pm 1.5 \cdot 10^{2})\,\mathrm{Oe}$, with the second stage of magnetometer we reached the sensitivity $\approx 8 \cdot 10^{-7}\,\mathrm{Gs/Hz^{1/2}}$ in the measurement range $(8 \cdot 10^{-7} - 2.5 \cdot 10^{-3})\,\mathrm{Oe}$. The accuracy and linearity of the output signal of the magnetometer were 0.01% and did not depend on the achieved sensitivity and the range of measured magnetic fields. The spatial resolution of the magnetometer was determined by the linear dimensions of the YBCO film twins, whose value at the field $H_{ic1} \approx 120.252\,\mathrm{Oe}$ was $\sim 300\,\mathrm{nm}$ and could decrease to 20 nm with H_{ic1} rise.

Funding

This study was financed from the budget under the state assignment.

Conflict of interest

The author declares that he has no conflict of interest.

References

[1] *Superconductor Applications: SQUIDs and Machines*. Ed. by B. B. Schwartz, S. Foner (Plenum Press, NY., 1977), v. 1.
[2] M.E. Limes, E.L. Foley, T.W. Kornack, S. Caliga, S. McBride, A. Braun, W. Lee, V.G. Lucivero, M.V. Romalis. Phys. Rev. Appl., **14**, 011002 (2020). DOI: 10.1103/PhysRevApplied.14.011002
[3] E.B. Aleksandrov, A.K. Vershovskii. Phys. Usp., **52**, 573 (2009). DOI: 10.3367/UFNr.0179.200906f.0605
[4] J.F. Barry, J.M. Schloss, E. Bauch, M.J. Turner, C.A. Hart, L.M. Pham, R.L. Walsworth. Rev. Mod. Phys., **92**, 015004 (2020). DOI: 10.1103/RevModPhys.92.015004
[5] S. Dushenko, K. Ambal, R.D. McMichael. Phys. Rev. Appl., **14**, 054036 (2020). DOI: 10.1103/PhysRevApplied.14.054036
[6] G.V. Karpov. Optoelectronics, Instrumentation and Data Processing, **51** (1), 58 (2015).
[7] R. Khasanov, Yu. Talanov, G. Teitel'baum. Phys. Rev. B, **54**, 13339 (1996). DOI: 10.1103/PhysRevB.54.13339
[8] B. Ando, S. Baglio, A.R. Bulsara, C. Trigona. Sensors and Actuators, **151**, 145 (2009). DOI: 10.1016/j.sna.2009.02.029
[9] Kh.R. Rostami. Instrum. Exp. Tech., **59** (2), 273 (2016). DOI: 10.1134/S0020441216010115
[10] V.K. Ignat'ev, A.A. Orlov, S.V. Perchenko, D.A. Stankevich. Tech. Phys. Lett., **43**, 687 (2017). DOI: 10.1134/S1063785017080090
[11] A. Oral, S.J. Bending, M. Henini. Appl. Phys. Lett., **69**, 1324 (1996). DOI: 10.1063/1.117582
[12] Kh.R. Rostami. Sbornik dokl. *XXVII Mezhdunarodnaya konferentsiya elektromagnitnoe pole i materialy* (*fundamental'nye fizicheskie issledovaniya*) (MEI, M., 2019), s. 536. (in Russian).
[13] K.R. Rostami, I.P. Nikitin. Measurement, **153**, 107423 (2020). DOI: 10.1016/j.measurement.2019.107423
[14] M. Eisterer. Phys. Rev. B, **99**, 094501 (2019). DOI: 10.1103/PhysRevB.99.094501
[15] Kh.R. Rostami. Int. J. Mod. Phys. B, **32** (31), 1850346 (2018). DOI: 10.1142/S0217979218503460
[16] Kh.R. Rostami. JETP Lett., **108** (11), 734 (2018). DOI: 10.1134/S0021364018230078
[17] Kh.R. Rostami. FTT, **64** (2), 149 (2022) (in Russian). DOI: 10.21883/FTT.2022.02.51945.107
[18] S. Nakahara, T. Boone, M.F. Yan, G.J. Fisanick, D.W. Johnson. J. Appl. Phys., **63**, 451 (1988). DOI: 10.1063/1.341149
[19] A.A. Abrikosov, A.I. Buzdin, M.L. Kulic, D.A. Kuptsov. Sov. Phys. JETP, **68** (1), 210 (1989).
[20] B. Kalisky, J.R. Kirtley, J.G. Analytis, J.-H. Chu, I.R. Fisher, K.A. Moler. Phys. Rev. B, **83**, 064511 (2011). DOI: 10.1103/PhysRevB.83.064511
[21] Kh.R. Ozmanyan, V.B. Sandomirskii, A.A. Sukhanov. Supercond. Sci. Technol., **3**, 255 (1990). DOI: 10.1088/0953-2048/3/5/008
[22] Paul Horowitz, Winfield Hill. *The ART of Electronics* (Cambridge University Press, Cambridge London NY., New Rochelle Melbourne Sydney, 1980), v. 1.
[23] Kh.R. Rostami. *Preoibrazovatel kod-tok*. Patent na izobretenie № 2007862, B.I. 1994. № 3. S. 1 (in Russian).
[24] Kh.R. Rostami. Tech. Phys., **65** (12), 1975 (2020). DOI: 10.1134/S1063784220120233
[25] V.V. Mantorov. Meas. Tech., **37** (4), 433 (1994). DOI: 10.1007/BF00981359
[26] V. Morosh, J. Linek, B. Müller, M.J. Martínez-Pérez, S. Wolter, T. Weimann, J. Beyer, T. Schurig, O. Kieler, A.B. Zorin, R. Kleiner, D. Koelle. Phys. Rev. Appl., **14**, 054072 (2020). DOI: 10.1103/PhysRevApplied.14.054072